

ResLPR: A LiDAR Data Restoration Network and Benchmark for Robust Place Recognition Against Weather Corruptions

Supplementary Material

Wenqing Kuang* Xiongwei Zhao* Yehui Shen Congcong Wen Huimin Lu Zongtan Zhou Xieyuanli Chen

I. RESLPRNET IMPLEMENTATION DETAILS

The architecture of ResLPRNet is introduced in the main text. Here, we provide a detailed overview of the input sizes and the number of input/output channels for each layer of ResLPRNet. The details are summarized in Table I. ResLPRNet comprises an initial convolutional layer, three encoder layers for downsampling, a transformer block for capturing global context, three decoder layers for upsampling, and a final convolutional layer to restore the output resolution. This architecture is designed to effectively balance feature extraction and resolution restoration, ensuring robust performance across different environments.

As described in the main text, the wavelet transform integrated into our model effectively isolates noise while preserving critical structural details in LiDAR range images. To further validate its robustness and generalization ability, Fig. 1 presents wavelet decomposition results under three distinct weather conditions from the WeatherKITTI and WeatherNCLT datasets. The low-frequency components (LL) retain the overall structures of the range images, while the high-frequency horizontal (LH), vertical (HL) and diagonal (HH) components effectively isolate noise. These results demonstrate the wavelet transform’s consistent performance across diverse datasets and challenging weather scenarios.

II. ADDITIONAL BENCHMARK DETAILS

In this paper, we simulate three types of weather corruptions: snow, fog, and rain. We employ LiDAR Fog Simulation [3] to model foggy conditions and LiDAR Light Scattering Augmentation [5] to simulate snowy and rainy conditions. The naturalness and authenticity of these simulators have been validated in previous studies [8], [7]. This section first provides the parameter settings of the simulators described in Section IV-B of the main text, followed by a detailed presentation of the statistical information for our proposed WeatherKITTI and WeatherNCLT datasets.

A. Parameter Configuration

As shown in Table II, the simulation parameters for various weather conditions are configured based on the type of LiDAR used in each dataset and the distribution of the corresponding point clouds. For fog simulation, both WeatherKITTI and WeatherNCLT share identical parameter settings. However, due to the skewed intensity distribution of point clouds in the NCLT dataset, where normalized values are predominantly concentrated in the upper range

TABLE I: Size of output size and input/output channels of each layer of ResLPRNet. WK and WN denote WeatherKITTI and WeatherNCLT, respectively.

Layer	Output Size		Input/C	Output/C
	WK	WN		
Initial Conv	64×1920	32×1440	2	2
Encoder1	64×1920	32×1440	2	48
Encoder2	32×960	16×720	48	96
Encoder3	16×480	8×360	96	192
Transformer	16×480	8×360	192	384
Decoder3	16×480	8×360	384	192
Decoder2	32×960	16×720	192	96
Decoder1	64×1920	32×1440	96	48
Final Conv	64×1920	32×1440	48	2

(0.9 to 1) rather than following a normal distribution, the parameter settings for snow and rain simulations in NCLT differ significantly from those in KITTI. These adjustments ensure a consistent noise point ratio across the two datasets under equivalent weather conditions.

B. Dataset Statistics

Ours proposed benchmark ResLPR contains two weather-corrupted datasets: WeatherKITTI and WeatherNCLT. WeatherKITTI is synthesized from the original point cloud data of sequences 00, 03 to 10 of the KITTI dataset, and each type of corruption and severity incorporates 52,317 frames of laser point cloud data. Concerning the WeatherNCLT dataset, we utilized the 2012-01-22 and 2012-02-12 sequences of the original NCLT dataset to simulate snowfall scenarios, generating 155,379 frames of point cloud data for each severity level. In the case of fog simulation, we processed the 2012-06-15 and 2012-08-04 sequences, obtaining 121,983 frames of corrupted point clouds for each severity level. Eventually, we synthesized 146,076 frames of point cloud data at the identical severity level for the simulation of rainy scenarios by employing the 2012-11-04 and 2012-11-16 sequences.

III. ADDITIONAL EXPERIMENTAL RESULTS

Here, we present the performance of the various LPR methods mentioned in Section V-C of the main text on the clean dataset, KITTI [2] and NCLT [1], as well as the experimental results under different weather conditions in WeatherKITTI and WeatherNCLT for both light and heavy severity levels. The main text currently highlights only the results for the mod severity level in Section V-C.

TABLE II: Configuration of weather simulation parameters based on LiDAR types, point cloud distribution, and weather severity levels

Weather	Severity Level	WeatherKITTI	WeatherNCLT
Fog Simulation	Light	fog simulation with $\beta = 0.008$	fog simulation with $\beta = 0.008$
	Moderate	fog simulation with $\beta = 0.05$	fog simulation with $\beta = 0.05$
	Heavy	fog simulation with $\beta = 0.2$	fog simulation with $\beta = 0.2$
Snow Simulation	Light	snowfall rate $r_s = 0.5$	snowfall rate $r_s = 50$
	Moderate	snowfall rate $r_s = 5$	snowfall rate $r_s = 400$
	Heavy	snowfall rate $r_s = 15$	snowfall rate $r_s = 2000$
Rain Simulation	Light	rain rate $r_r = 15$	rain rate $r_r = 4000$
	Moderate	rain rate $r_r = 50$	rain rate $r_r = 6000$
	Heavy	rain rate $r_r = 150$	rain rate $r_r = 8000$

A. Results on Different Levels of Corruption

Clean Dataset Performance: We assessed three distinct LPR methods on our benchmark. For the traditional LPR method, SC [6], we utilized its open-source implementation to replicate results on the KITTI [2] and NCLT [1] datasets. For CVTNet [10], we reproduced its results on the KITTI dataset and directly used the pretrained model provided by the authors to conduct experiments on the NCLT dataset. We trained LPSNet [9] following the protocol of CVTNet on the KITTI and NCLT datasets for subsequent evaluation.

In the clean datasets, the performance of three LPR methods is presented in Table III. It is evident that CVTNet demonstrates the best overall performance across both datasets, particularly excelling on the NCLT dataset, where its performance significantly surpasses that of SC and LPSNet across all sequences. For instance, in the sequence with the largest time span, 2012-11-16, CVTNet maintains a Recall@1 of 0.790, while the corresponding metrics for the other two methods drop to around 0.5. Regarding the performance of LPSNet, it shows competitive results in the Recall@5 metric on the KITTI dataset and the Recall@20 metric on the NCLT dataset. As for the traditional LPR method, SC, its performance in both datasets is comparable to that of LPSNet.

Light Corruption Performance: Here, we present more experimental results of using different preprocessing methods with LPR methods on WeatherKITTI and WeatherNCLT at light severity level in Tables IV and V, respectively. As shown, the performance of the three LPR methods under light weather conditions is higher than under moderate severity levels but still exhibits a notable decline. Consistent with the findings in the main text, all LPR methods show substantial improvement when our proposed ResLPRNet is applied, significantly outperforming the other two preprocessing methods. For example, in the case of KITTI snow corruption, the AUC for CVTNet does not exceed 0.1 after preprocessing with WeatherNet or TripleMixer. However, after restoration using ResLPRNet, the AUC improves dramatically to 0.665. This demonstrates that while LPR methods remain vulnerable to even light corruption, ResLPRNet effectively enhances their robustness and performance under such conditions.

Heavy Corruption Performance: In Table VI, we report the performance of the LPR method with three preprocessing

techniques under heavy corruption in WeatherKITTI. The corresponding results on WeatherNCLT are presented in Table VII. The experimental results indicate that despite heavy corruption, our proposed ResLPRNet continues to function effectively, significantly enhancing the performance of the LPR method under extreme conditions and maintaining a certain level of robustness across different severity levels of corruption. For instance, during heavy rain in WeatherKITTI, the AUC, when combined with the SC algorithm of the restoration network, still reaches 0.807. Similarly, in the severely corrupted snowy conditions of WeatherNCLT, the Recall@1 of CVTNet, after applying ResLPRNet, improves from a complete failure under corrupted conditions to as high as 0.898, consistently maintaining this level across three different severity levels.

IV. ADDITIONAL VISUALIZATION

A. Visualization of Corruption

As shown in Fig. 2, we present the point clouds with different levels of corruption for WeatherKITTI and WeatherNCLT of the proposed benchmark. As illustrated, the point clouds in snowy scenarios are relatively sparse, with fewer points lost compared to foggy weather. In contrast, the simulated foggy scenarios exhibit a significant increase in point cloud loss as the severity level increases. For the rainy weather scenario, the noise points are more concentrated compared to both snow and fog, leading to a substantial loss of point clouds as well.

B. Visualization of Preprocessing Methods

we apply two point cloud denoising methods alongside our proposed restoration network to enhance the performance of the LPR method under corrupted point cloud conditions. As illustrated in Fig. 3, we visualize the point clouds obtained after processing the corrupted point clouds with the three preprocessing methods. Specifically, the point clouds restored by our proposed ResLPRNet demonstrate a significant recovery of the main geometric structures, distinguishing them from the point clouds produced by the denoising methods. For instance, in the foggy weather scenario of the WeatherKITTI dataset, the restoration network successfully recovers the entire intersection point cloud, while the denoising network is limited to merely removing noise points. Similarly, in the

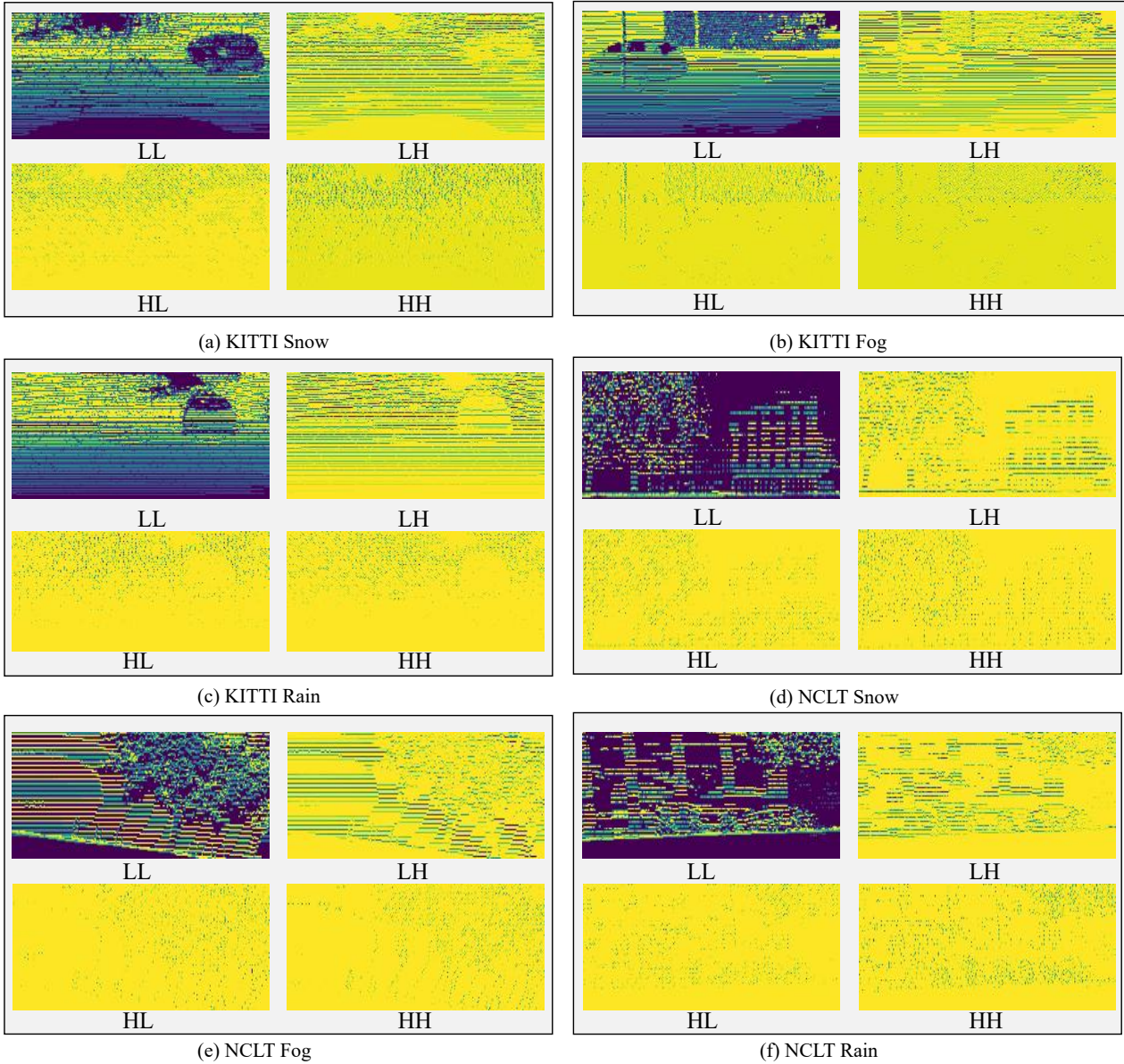


Fig. 1: Visualization of the wavelet transform in our model across diverse datasets and weather scenarios. LL represent overall low-frequency components, while LH, HL and HH correspond to horizontal, vertical and diagonal high-frequency components.

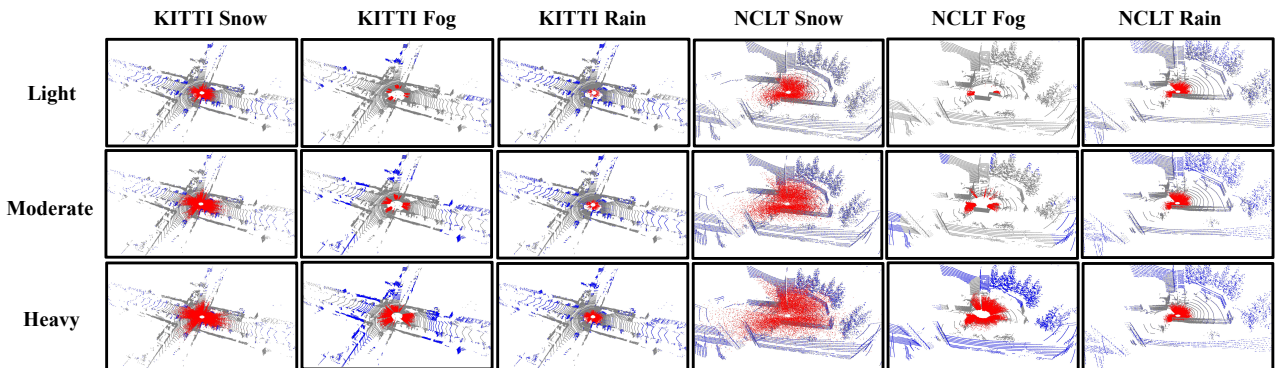


Fig. 2: Visualization of corrupted point clouds of varying severity in WeatherKITTI and WeatherNCLT. The red points in the point cloud signify the noise points, and the blue points denote the lost points.

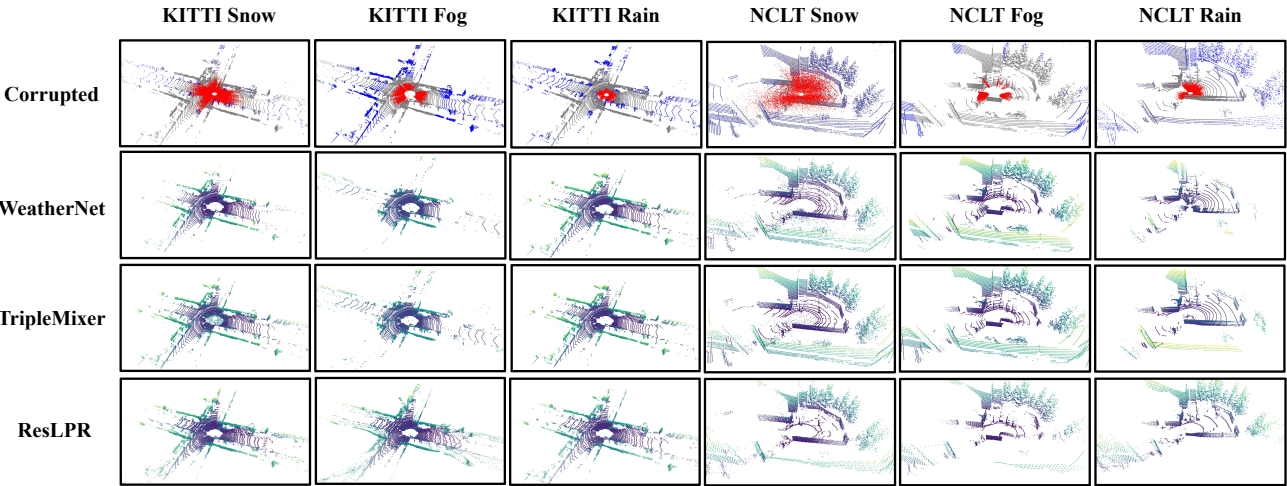


Fig. 3: Visualization of point clouds processed by three different preprocessing methods. In the corrupted point clouds, **red points** represent noise points, and **blue points** represent lost points.

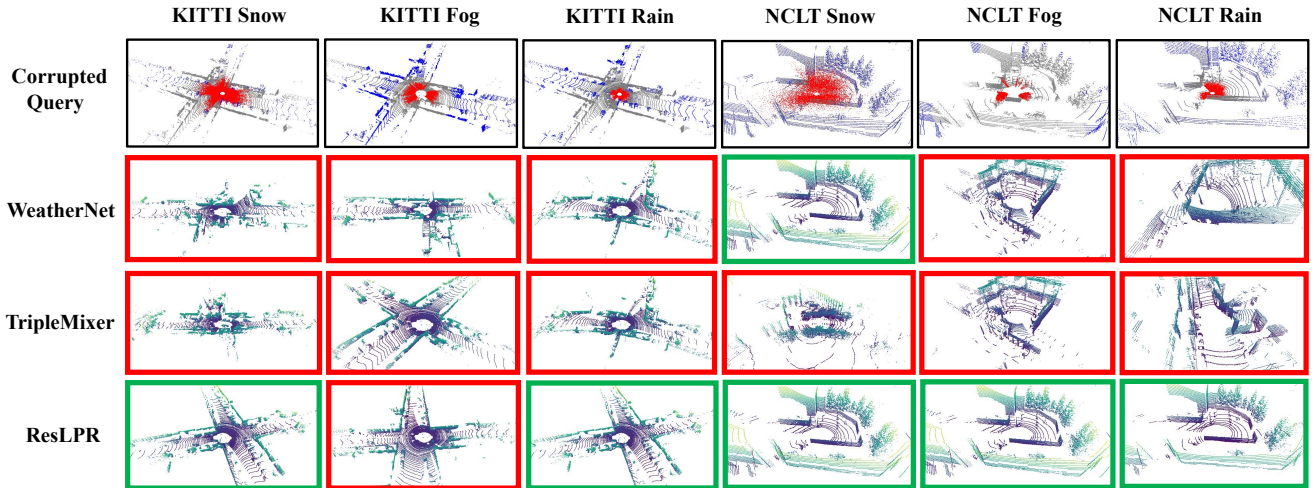


Fig. 4: Qualitative visualizations of some corruption query examples, along with their top-1 retrieved matches on the WeatherKITTI and WeatherNCLT datasets using SC. In the corrupted query point clouds, the **red points** in the point cloud signify the noise points, and the **blue points** denote the lost points. **red boxes** indicate incorrect retrieval results, while **green boxes** denote correct retrievals.

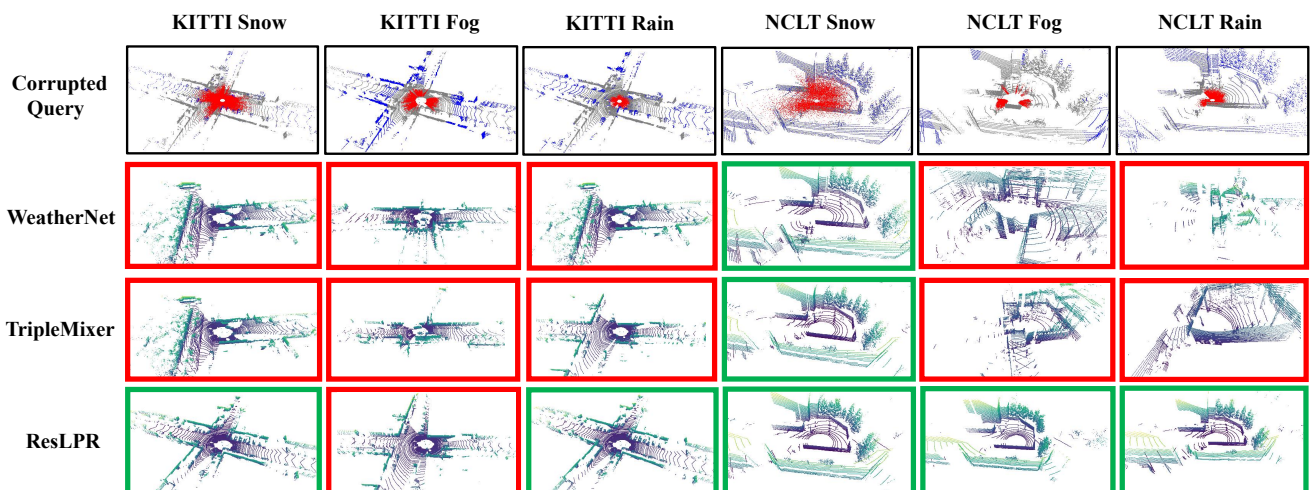


Fig. 5: Qualitative visualizations of some corruption query examples, along with their top-1 retrieved matches on the WeatherKITTI and WeatherNCLT datasets using LPSNet. In the corrupted query point clouds, the **red points** in the point cloud signify the noise points, and the **blue points** denote the lost points. **red boxes** indicate incorrect retrieval results, while **green boxes** denote correct retrievals.

TABLE III: The performance of LPR methods on original KITTI and NCLT.

LPR		KITTI 00				NCLT 2012-02-12			NCLT 2012-06-15			NCLT 2012-11-16		
Method		AUC↑	F1↑	R@1↑	R@5↑	R@1↑	R@5↑	R@20↑	R@1↑	R@5↑	R@20↑	R@1↑	R@5↑	R@20↑
SC	0.852	0.840	0.827	0.861	0.881	0.896	0.907	0.722	0.730	0.734	0.582	0.607	0.625	
CVTNet	0.875	0.836	0.853	0.876	0.916	0.948	0.972	0.829	0.891	0.935	0.790	0.862	0.910	
LPSNet	0.667	0.652	0.849	0.879	0.647	0.781	0.831	0.473	0.660	0.748	0.493	0.630	0.707	

TABLE IV: The benchmark results of LPR methods with three preprocessing methods under light corruption condition on WeatherKITTI.

Method		mSR _l ↑	KITTI Snow				KITTI Fog				KITTI Rain			
Preprocessing	LPR	AUC↑	F1↑	R@1↑	R@5↑	AUC↑	F1↑	R@1↑	R@5↑	AUC↑	F1↑	R@1↑	R@5↑	
Corruption	SC [6]	0.310	0.155	0.203	0.166	0.188	0.580	0.602	0.537	0.562	0.206	0.241	0.214	0.251
	CVTNet [10]	0.192	0.041	0.077	0.116	0.202	0.327	0.339	0.394	0.481	0.113	0.158	0.224	0.340
	LPSNet [9]	0.360	0.076	0.130	0.264	0.388	0.266	0.329	0.554	0.615	0.199	0.271	0.508	0.667
WeatherNet[4]	SC [6]	0.424	0.321	0.375	0.294	0.307	0.559	0.596	0.497	0.527	0.456	0.501	0.421	0.439
	CVTNet [10]	0.112	0.011	0.027	0.040	0.082	0.097	0.142	0.175	0.232	0.107	0.153	0.212	0.331
	LPSNet [9]	0.418	0.144	0.199	0.335	0.468	0.205	0.285	0.461	0.557	0.347	0.367	0.585	0.727
TripleMixer[11]	SC [6]	0.496	0.215	0.255	0.223	0.253	0.717	0.729	0.677	0.702	0.480	0.526	0.434	0.447
	CVTNet [10]	0.226	0.072	0.115	0.180	0.292	0.379	0.382	0.437	0.500	0.121	0.166	0.231	0.346
	LPSNet [9]	0.551	0.276	0.328	0.532	0.671	0.307	0.380	0.597	0.691	0.346	0.369	0.616	0.735
ResLPR(Ours)	SC [6]	0.949	0.815	0.782	0.811	0.845	0.807	0.783	0.797	0.834	0.820	0.804	0.812	0.839
	CVTNet [10]	0.794	0.665	0.582	0.825	0.873	0.409	0.382	0.712	0.830	0.777	0.707	0.848	0.890
	LPSNet [9]	0.915	0.547	0.567	0.832	0.875	0.505	0.562	0.825	0.859	0.549	0.586	0.829	0.880

TABLE V: The benchmark results of LPR methods with three preprocessing methods under light corruption condition on WeatherNCLT.

Method		mSR _p ↑	NCLT Snow			NCLT Fog			NCLT Rain		
Preprocessing	LPR	R@1↑	R@5↑	R@20↑	R@1↑	R@5↑	R@20↑	R@1↑	R@5↑	R@20↑	
Corruption	SC [6]	0.148	0.135	0.150	0.166	0.103	0.112	0.117	0.089	0.109	0.125
	CVTNet [10]	0	-	-	0.004	-	-	-	-	-	0.004
	LPSNet [9]	0.187	0.212	0.311	0.399	0.049	0.059	0.073	0.079	0.096	0.112
WeatherNet[4]	SC [6]	0.225	0.356	0.374	0.390	0.115	0.121	0.125	0.097	0.115	0.130
	CVTNet [10]	0.380	0.787	0.845	0.891	0.253	0.308	0.361	0.058	0.082	0.111
	LPSNet [9]	0.205	0.240	0.357	0.449	0.047	0.059	0.007	0.072	0.093	0.105
TripleMixer[11]	SC [6]	0.159	0.150	0.165	0.180	0.116	0.123	0.129	0.096	0.116	0.131
	CVTNet [10]	0.419	0.835	0.889	0.933	0.254	0.309	0.362	0.096	0.127	0.151
	LPSNet [9]	0.224	0.272	0.395	0.487	0.046	0.062	0.073	0.080	0.103	0.116
ResLPR(Ours)	SC [6]	0.705	0.647	0.669	0.683	0.684	0.696	0.702	0.328	0.361	0.394
	CVTNet [10]	0.920	0.896	0.935	0.960	0.796	0.864	0.917	0.605	0.717	0.804
	LPSNet [9]	0.921	0.662	0.764	0.813	0.543	0.702	0.781	0.331	0.466	0.563

rain scenario of the WeatherNCLT dataset, the restored point cloud effectively recovers the point cloud of the trees on the right side of the scene, ensuring that the relative integrity of the main geometric structures is maintained.

C. Visualization of LPR Methods

In the main text, we present the visualization results of the CVTNet after applying three preprocessing methods. Here, we further showcase the visualization results of SC [6] and LPSNet [9] in Fig. 4 and Fig. 5 respectively. As illustrated, in the visualization results of SC, after applying our restoration network, correct matches were successfully retrieved in all scenarios except for the most severe fog conditions in the WeatherKITTI dataset. In contrast, when observing the matching results under the other two denoising methods, only the WeatherNet [4] method achieved a successful match once in the snow weather condition of the WeatherNCLT dataset. For the visualization results of LPSNet, the top-1 matching success rate after applying ResLPRNet was significantly higher than the correct matching counts corresponding to the

two denoising methods. After preprocessing the corrupted point clouds with the two denoising methods, successful matches were only achieved in the snow scenario of the WeatherNCLT dataset.

REFERENCES

- [1] N. Carlevaris-Bianco, A.K. Ushani, and R.M. Eustice. University of michigan north campus long-term vision and lidar dataset. *The International Journal of Robotics Research*, 35(9):1023–1035, 2016.
- [2] A. Geiger, P. Lenz, and R. Urtasun. Are we ready for autonomous driving? the kitti vision benchmark suite. In *2012 IEEE conference on computer vision and pattern recognition*, pages 3354–3361. IEEE, 2012.
- [3] M. Hahner, C. Sakaridis, D. Dai, and L. Van Gool. Fog simulation on real lidar point clouds for 3d object detection in adverse weather. In *Proceedings of the IEEE/CVF international conference on computer vision*, pages 15283–15292, 2021.
- [4] R. Heinzler, F. Pieck, P. Schindler, and W. Stork. Cnn-based lidar point cloud de-noising in adverse weather. *IEEE Robotics and Automation Letters*, 5(2):2514–2521, 2020.
- [5] V. Kilic, D. Hegde, V. Sindagi, A.B. Cooper, M.A. Foster, and V.M. Patel. Lidar light scattering augmentation (lisa): Physics-based simulation of adverse weather conditions for 3d object detection. *arXiv preprint arXiv:2107.07004*, 2021.

TABLE VI: The benchmark results of LPR methods with three preprocessing methods under heavy corruption condition on WeatherKITTI.

Method		mSR _i ↑	KITTI Snow				KITTI Fog				KITTI Rain			
Preprocessing	LPR		AUC↑	F1↑	R@1↑	R@5↑	AUC↑	F1↑	R@1↑	R@5↑	AUC↑	F1↑	R@1↑	R@5↑
Corruption	SC [6]	0.310	0.119	0.159	0.139	0.161	0.294	0.335	0.276	0.294	0.178	0.211	0.194	0.221
	CVTNet [10]	0.192	0.020	0.041	0.065	0.124	0.095	0.130	0.144	0.214	0.068	0.112	0.156	0.255
	LPSNet [9]	0.360	0.028	0.055	0.100	0.163	0.103	0.155	0.239	0.316	0.162	0.231	0.413	0.580
WeatherNet[4]	SC [6]	0.424	0.216	0.264	0.194	0.208	0.277	0.320	0.238	0.256	0.407	0.457	0.372	0.382
	CVTNet [10]	0.112	0.004	0.014	0.015	0.037	0.023	0.046	0.052	0.093	0.062	0.103	0.151	0.240
	LPSNet [9]	0.418	0.073	0.116	0.211	0.313	0.080	0.138	0.191	0.269	0.277	0.312	0.497	0.655
TripleMixer[11]	SC [6]	0.496	0.150	0.185	0.168	0.186	0.514	0.545	0.469	0.492	0.425	0.476	0.385	0.392
	CVTNet [10]	0.226	0.036	0.070	0.109	0.182	0.123	0.159	0.173	0.227	0.076	0.121	0.168	0.266
	LPSNet [9]	0.551	0.194	0.247	0.410	0.566	0.140	0.180	0.301	0.403	0.306	0.337	0.526	0.667
ResLPR(Ours)	SC [6]	0.949	0.790	0.755	0.787	0.827	0.768	0.731	0.774	0.815	0.807	0.787	0.796	0.834
	CVTNet [10]	0.794	0.553	0.486	0.775	0.853	0.353	0.340	0.693	0.819	0.699	0.620	0.833	0.884
	LPSNet [9]	0.915	0.526	0.557	0.823	0.871	0.500	0.550	0.817	0.861	0.541	0.570	0.815	0.869

TABLE VII: The benchmark results of LPR methods with three preprocessing methods under heavy corruption condition on WeatherNCLT.

Method		mSR _p ↑	NCLT Snow			NCLT Fog			NCLT Rain		
Preprocessing	LPR		R@1↑	R@5↑	R@20↑	R@1↑	R@5↑	R@20↑	R@1↑	R@5↑	R@20↑
Corruption	SC [6]	0.148	0.119	0.135	0.148	0.064	0.074	0.077	0.082	0.099	0.113
	CVTNet [10]	0	-	-	0.004	-	-	-	-	-	0.004
	LPSNet [9]	0.187	0.147	0.208	0.281	0.033	0.042	0.049	0.064	0.085	0.103
WeatherNet[4]	SC [6]	0.225	0.275	0.293	0.310	0.064	0.071	0.075	0.084	0.102	0.118
	CVTNet [10]	0.380	0.599	0.684	0.756	0.109	0.134	0.159	0.051	0.070	0.101
	LPSNet [9]	0.205	0.168	0.253	0.338	0.032	0.045	0.054	0.065	0.083	0.096
TripleMixer[11]	SC [6]	0.159	0.133	0.146	0.161	0.064	0.071	0.075	0.088	0.107	0.121
	CVTNet [10]	0.419	0.719	0.799	0.864	0.109	0.136	0.161	0.080	0.105	0.131
	LPSNet [9]	0.224	0.189	0.278	0.368	0.033	0.042	0.054	0.068	0.089	0.106
ResLPR(Ours)	SC [6]	0.705	0.559	0.580	0.598	0.522	0.539	0.546	0.317	0.347	0.377
	CVTNet [10]	0.920	0.898	0.935	0.957	0.743	0.825	0.891	0.590	0.706	0.794
	LPSNet [9]	0.921	0.651	0.756	0.807	0.492	0.650	0.744	0.325	0.456	0.553

- [6] G. Kim and A. Kim. Scan context: Egocentric spatial descriptor for place recognition within 3d point cloud map. In *2018 IEEE/RSJ International Conference on Intelligent Robots and Systems (IROS)*, pages 4802–4809. IEEE, 2018.
- [7] L. Kong, Y. Liu, X. Li, R. Chen, W. Zhang, J. Ren, L. Pan, K. Chen, and Z. Liu. Robo3d: Towards robust and reliable 3d perception against corruptions. In *Proceedings of the IEEE/CVF International Conference on Computer Vision*, pages 19994–20006, 2023.
- [8] S. Li, Z. Wang, F. Juefei-Xu, Q. Guo, X. Li, and L. Ma. Common corruption robustness of point cloud detectors: Benchmark and enhancement. *IEEE Transactions on Multimedia*, 2023.
- [9] C. Liu, G. Chen, and R. Song. Lps-net: Lightweight parameter-shared network for point cloud-based place recognition. In *2024 IEEE International Conference on Robotics and Automation (ICRA)*, pages 448–454. IEEE, 2024.
- [10] J. Ma, G. Xiong, J. Xu, and X. Chen. Cvtnet: A cross-view transformer network for lidar-based place recognition in autonomous driving environments. *IEEE Transactions on Industrial Informatics*, 2023.
- [11] X. Zhao, C. Wen, Y. Wang, H. Bai, and W. Dou. Triplemixer: A 3d point cloud denoising model for adverse weather. *arXiv preprint arXiv:2408.13802*, 2024.